PCCP

Cite this: *Phys. Chem. Chem. Phys.*, 2011, **13**, 3161–3170

www.rsc.org/pccp

PAPER

Small-angle scattering from phospholipid nanodiscs: derivation and refinement of a molecular constrained analytical model form factor†

Nicholas Skar-Gislinge and Lise Arleth*

Received 3rd July 2010, Accepted 1st November 2010
DOI: 10.1039/c0cp01074j

Nanodiscs™ consist of small phospholipid bilayer discs surrounded and stabilized by amphiphilic protein belts. Nanodiscs and their confinement and stabilization of nanometer sized pieces of phospholipid bilayer are highly interesting from a membrane physics point of view. We demonstrate how the detailed structure of Di-Lauroyl-Phosphatidyl Choline (DLPC) nanodiscs may be determined by simultaneous fitting of a structural model to small-angle scattering data from the nanodiscs as investigated in three different contrast situations, respectively two SANS contrasts and one SAXS contrast. The article gives a detailed account of the underlying structural model for the nanodiscs and describe how additional chemical and biophysical information can be incorporated in the model in terms of molecular constraints. We discuss and quantify the contribution from the different elements of the structural model and provide very strong experimental support for the nanodiscs as having an elliptical cross-section and with poly-histidine tags protruding out from the rim of the protein belt. The analysis also provides unprecedented information about the structural conformation of the phospholipids when these are localized in the nanodiscs. The model paves the first part of the way in order to reach our long term goal of using the nanodiscs as a platform for small-angle scattering based structural investigations of membrane proteins in solution.

Introduction

The quality of the experimental data obtained at modern SAXS and SANS facilities has improved steadily throughout the last decades. This is a natural result of the increase in both neutron and, in particular, X-ray flux as well as a result of a continuous specialization of both instruments and beam-line scientists. One of the consequences of this is that so-called "Bio-SAXS" instruments are being established at more and more large scale synchrotron X-ray facilities. A Bio-SAXS is characterized by having a relatively fixed experimental configuration which is optimized for weakly scattering biomolecules in solution. This includes for example samples placed in a fixed flow-through cuvette and unbroken vacuum from the beginning of the collimation section to the detector. The high quality data that may be obtained from these instruments opens up for extracting much more detailed information from SAXS and SANS data than previously possible. In order to make the most of these data, a similar development is therefore required for the development of the data analysis methods. With this article we wish to provide an example of such a method development.

Biophysics, Faculty of Life Sciences, University of Copenhagen, Denmark. E-mail: lia@life.ku.dk

† This article was submitted as part of a special collection on scattering methods applied to soft matter, marking the 65th birthday of Professor Otto Glatter.

We demonstrate that by combining data from state of the art SAXS and SANS instruments with a state of the art approach to the data analysis we can determine the solution structure of a complex biomolecular system in unprecedented detail. Besides from combining SAXS and SANS, the approach builds on the inclusion of so-called molecular constraints; *i.e.* the inclusion of information available from other sources, *e.g.* information about the chemical composition of the building blocks of the sample along with biophysical information such as sample concentration, partial specific densities of the single components *etc.*

The test case of this presented model development is the so-called phospholipid nanodisc system. Nanodisc's[1] are amphilic self-assembled particles consisting of an phospholipid bilayer disc which is stabilized by a "belt" constituted by two amphiphilic membrane scaffold proteins (MSP's). The amino-acid sequence of the MSP defines the length of the belt, which again fully controls the outer diameter of the formed nanodisc. Typical diameters of the nanodiscs are from 10 nm to 14 nm.[2,3] While the nanodisc system is highly interesting on its own right from a membrane physics point-of-view, the major broader interest in the system is related to the applicability and large potential of the system as a custom-fitted, nanometer-sized sample holder for membrane proteins.[4–6] The MSP, *i.e.* the protein belt, is inspired from the high density lipoprotein (HDL)-system, Apo-A1, and may be seen as a version of this that is genetically optimised towards the formation of circular discs.[2,3,7]

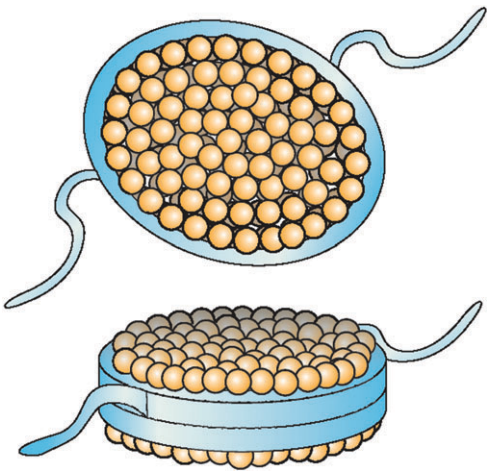

Fig. 1 Illustration of the nanodisc structure according to ref. 8. The cross-section is elliptical and the histidine-tags of the MSP's are visible on the outer rim of the belt.

In a recent publication[8] we have reported a detailed small-angle scattering study of nanodiscs formed with, respectively, Di-Lauroyl Phosphatidyl Choline (DLPC) and Palmitoyl-Oleoyl Phosphatidyl Choline (POPC) and in the temperature range from 1 °C to 20 °C. In the study we combined small-angle neutron scattering (SANS) and small-angle X-ray scattering (SAXS). We found an elliptical shape of the nanodiscs and showed that the histidine-tags of the MSP-belts are clearly visible in the nanodisc structure and protruding out from the outer rim of the MSP-belt that stabilizes the nanodiscs. The obtained structure for the nanodiscs is illustrated in Fig. 1. We showed that the MSP-belt and its temperature dependence is the main decisive factor for both the overall shape of the nanodiscs and for the packing of the phospholipids. We found that POPC becomes laterally expanded when localized in nanodiscs, leading to a relative thinning of the phospholipid membrane as compared to their structural state in unilamellar liposomes. Whereas the opposite is the case for the relatively short-chain DLPC, which becomes laterally compressed and have a slightly more thick hydrophobic bilayer in the nanodiscs. We propose that this, respectively the lateral expansion of POPC and the lateral compression of DLPC, is a consequence of the minimization of the hydrophobic mismatch[9] between the hydrophobic inside of the MSP-belt and the hydrophic sides of the encircled phospholipid bilayer disc.

The combined SANS and SAXS structural study of the nanodisc system is totally dependent on a sufficiently good and detailed structural model for the nanodiscs system. This includes the careful incorporation of molecular information about the molecular building blocks as obtained by complementary biophysical techniques, such as high precision densitometry and determination of sample concentrations. In the present article, we will therefore take the opportunity to explain the underlying model in full detail and evaluate the quantitative effect of the different elements of the model, both in terms of the differential scattering cross-sections, that are directly determined in a SAXS or SANS experiment, and in terms of the direct space pair-distance distribution functions that may be determined by indirect Fourier transform of the scattering data.[10]

We will show how the systematic incorporation of molecular information, in terms of so-called, molecular constraints, along with the simultaneous fitting of three small-angle scattering contrasts on the same sample, two SANS contrast and one SAXS contrast, allow us to minimize the number of free parameters in the structural model and use the combined set of experimental data to determine the structure of the nanodiscs in a so far, unprecedented detail. While cryo-TEM shows potential for providing structural information at comparable resolution,[11] small-angle scattering has the great advantage of being a solution based technique which requires very little prior sample preparation and which allows for easy accessible systematic investigations under a range of variable external conditions, including variable temperature, ion-strength and hydrostatic pressure, and which, in the case of synchrotron-SAXS, allows for ultra fast time-resolved studies.

Theory and mathematical modeling

General introduction to small-angle scattering from particles in solution

For an isotropic sample of particles in solution, the small-angle scattering experiment produces a centrosymetric scattering pattern. The elastically scattered intensity is usually described as a function of the scattering vector q, which is again related to the scattering angle, 2θ *via* the wave length of the incoming photon-beam (SAXS) or the neutron beam (SANS) the following way: $q = 4\pi \sin(\theta)/\lambda$. The small-angle scattering from particles in solution may then be described as the product of a form factor and a structure factor. According to commonly accepted nomenclature within small-angle scattering,[12] the form factor describes the intra-particle interference of the scattered photons or neutrons, and therefore contain information on the shape of the single particles, whereas the structure factor describes the inter-particle interference and contains information on particle–particle interactions within in the sample. For very dilute samples, the particle–particle interactions are negligible, the structure factor may be set to unity, and the q-dependent differential scattering cross section per unit volume becomes:

$$\frac{d\Sigma\ (q)}{d\Omega} = n(\Delta b)^2 P(q) \qquad (1)$$

where n is the particle number density, *i.e.* the number of particles per unit volume and Δb is the excess scattering length of the single particles. This entity is generally defined as $\Delta b = V \times (\rho - \rho_0)$, where V is the volume of the particle, ρ is the average scattering length density of the particle calculated as $\rho = \sum b_i / \sum v_i$, where the v_i's denote the volumes of the different parts of the particle and the b_i's denote the corresponding scattering lengths. ρ_0 is the average scattering length density of the solvent. More details on the calculation of Δb will be provided later. $P(q)$ is the form factor and describes the q-dependence of the scattering. In this presentation, $P(q)$ is normalized so that $P(0) = 1$. The form factor can in principle be calculated for any given shape *via*

the Fourier transformation of the excess scattering length density function, $\Delta\rho(\mathbf{r})$.

$$P(\mathbf{q}) = \frac{1}{\Delta b^2}\left|\int_v \rho(\mathbf{r})\mathrm{e}^{-i\mathbf{q}\cdot\mathbf{r}}\mathrm{d}\mathbf{r}\right|^2 = |\psi(\mathbf{q})|^2 \qquad (2)$$

where $\psi(\mathbf{q})$ denotes the so-called form factor amplitude. A large number of analytical and semi analytical form factors, for a wide range of geometrical objects are available in the literature.[13,14]

The above mentioned structure factor, on the other hand is somewhat more complicated to calculate and only exists as an analytical expression in a few cases. In this study, care has been taken to work in the dilute regime where the inter-particle interactions are weak and the structure factor effects become negligible.

The basic building block for the nanodisc form factor

Nanodiscs are expected to have a local cylindrical geometry and the form factor for nanodiscs was constructed using the form factor for a cylinder with an elliptical cross section as the basic building block:

$$\psi_{\mathrm{cyl}}(q,\alpha,\phi,r,L) = \frac{2J_1(qr(\phi)\sin(\alpha))}{qr(\phi)\sin(\alpha)}\frac{\sin(qL\cos(\alpha)/2)}{qL\cos(\alpha)/2} \qquad (3)$$

where J_1 is the first order Bessel function, α the azimuthal angle, L is the cylinder height and r the cylinder radius as a function of horizontal angle ϕ and the long and short half axis of the elliptical cross section, a and b: $r(\phi) = \sqrt{a^2\sin^2(\phi) + b^2\cos^2(\phi)}$ (see Fig. 2).

As illustrated in Fig. 3 the form factor of different objects may be combined to yield form factors of even more complicated objects, this is the basic principle used in this work.

The phospholipid interior. The phospholipid bilayer interior of the nanodisc is represented by a stack of cylinders with elliptical cross section where the top and bottom cylinders represent the hydrophilic phospholipid head group region. In between these two head group layers, the hydrophobic alkyl chain region is represented by a pair of cylinders corresponding to the top and bottom alkyl chain layer. A third layer representing the methyl end groups of the lipid tails is sandwiched in between these two alkyl chain layers. The scattering amplitude can be written as the sum of the form factor amplitudes for each cylinder weighted by their respective scattering lengths (see Fig. 4). The total scattering amplitude of this stack, A_{stack}, becomes:

$$A_{\mathrm{stack}} = A_{\mathrm{heads}} + A_{\mathrm{alkyl}} + A_{\mathrm{methyl}} = \Delta b_{\mathrm{heads}}\psi_{\mathrm{heads}} + \Delta b_{\mathrm{alkyl}}\psi_{\mathrm{alkyl}} + \Delta b_{\mathrm{methyl}}\psi_{\mathrm{methyl}} \qquad (4)$$

where the ψ's are the form factor amplitudes and the Δb's are the scattering lengths for the different units taken with respect to the aqueous solvent.

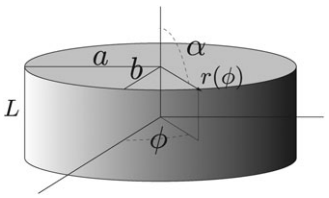

Fig. 2 Cylinder with an elliptical cross section.

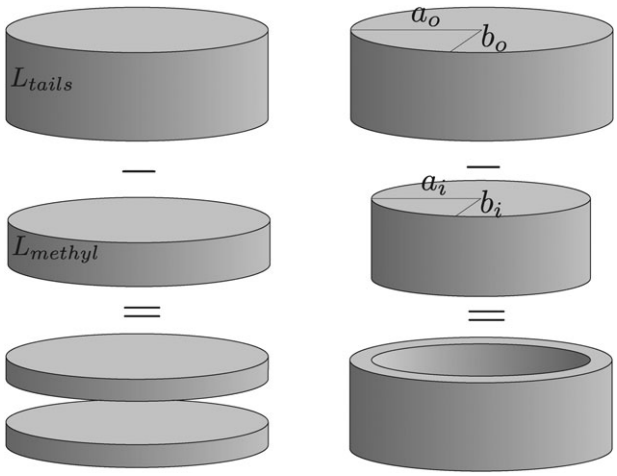

Fig. 3 Principle of combining form factors to yield more complex form factors.

The methyl groups in the center are represented by a single elliptical cylinder, with the form factor amplitude, ψ_{methyl}, calculated using eqn (3), where a and b is now the long and short axis of the lipid bilayer and L_{methyl} is the height of the methyl groups:

$$\psi_{\mathrm{methyl}} = \psi_{\mathrm{cyl}}(q,\alpha,\phi,r,L_{\mathrm{methyl}}) \qquad (5)$$

The alkyl chains of the lipids are represented by a cylinder with the same height as the tail groups, however with the volume corresponding to the methyl groups subtracted, this is sketched in Fig. 3. The form factor amplitude, ψ_{alkyl}, becomes:

$$\psi_{\mathrm{alkyl}} = \frac{(L_{\mathrm{tails}}\psi_{\mathrm{cyl}}(q,\alpha,\phi,r,L_{\mathrm{tails}}) - L_{\mathrm{methyl}}\psi_{\mathrm{methyl}})}{L_{\mathrm{alkyl}}} \qquad (6)$$

where $L_{\mathrm{alkyl}} = L_{\mathrm{tails}} - L_{\mathrm{methyl}}$ and where L_{tails} is the total height of the hydrophobic tails including the methyl group layer. The same approach is used to create form factor amplitude from the pair of cylinders representing the phospholipid head groups, ψ_{heads}: These are represented by a cylinder of the total height of the bilayer minus the combined volume taken up by the tails including the methyl groups:

$$\psi_{\mathrm{heads}} = \frac{(L_{\mathrm{total}}\psi_{\mathrm{cyl}}(q,\alpha,\phi,r,L_{\mathrm{total}}) - L_{\mathrm{tails}}\psi_{\mathrm{cyl}}(q,\alpha,\phi,r,L_{\mathrm{tails}}))}{L_{\mathrm{heads}}} \qquad (7)$$

where, $L_{\mathrm{heads}} = L_{\mathrm{total}} - L_{\mathrm{tails}}$. L_{total} is the total height of the bilayer. Note that r should be taken as a function of a, b and ϕ in eqn (7), eqn (6) and (7) as described in the comments to eqn (3).

The protein belt. The protein belt stabilizing the phospholipid bilayer is represented as a hollow cylinder. In order to calculate the corresponding scattering amplitude, A_{belt}, we combine the form factor amplitudes from two elliptical cylinders with a_o and b_o as the outer, and a_i and b_i as the inner half axes (See Fig. 3 (right)):

$$A_{\mathrm{belt}} = \Delta b_{\mathrm{belt}}\frac{L_{\mathrm{belt}}\pi(R_o^2\psi_{\mathrm{cyl}}(q,\alpha,\phi,R_o,L_{\mathrm{belt}}) - R_i^2\psi_{\mathrm{cyl}}(q,\alpha,\phi,R_i,L_{\mathrm{belt}}))}{V_{\mathrm{belt}}} = \Delta b_{\mathrm{belt}}\psi_{\mathrm{belt}} \qquad (8)$$

where R_o and R_i are the outer and inner radii. Again both are functions of the horizontal angle ϕ so that: $R_i(\phi) = \sqrt{a_i^2 \sin^2(\phi) + b_i^2 \cos^2(\phi)}$ and $R_o(\phi) = \sqrt{a_o^2 \sin^2(\phi) + b_o^2 \cos^2(\phi)}$. The pairs of axis ratios (a_i,b_i) and (a_o,b_o) are chosen such that $a_o - a_i = b_o - b_i$, such that we have approximately the same belt thickness for different ϕ-values.

Assembling the form factor for the nanodisc. As illustrated in Fig 4, the scattering amplitudes from the phospholipid bilayer and the protein belt can be combined to produce the total scattering amplitude of the nanodisc, A_{nd}, which using eqn (8) and (4) becomes:

$$A_{nd} = \Delta b_{nd}\psi_{nd} = \Delta b_{nd} \times \left(\frac{\Delta b_{\text{belt}}\psi_{\text{belt}} + \Delta b_{\text{heads}}\psi_{\text{heads}} + \Delta b_{\text{alkyl}}\psi_{\text{alkyl}} + \Delta b_{\text{methyl}}\psi_{\text{methyl}}}{\Delta b_{nd}}\right) \quad (9)$$

Referring to eqn (1), the differential scattering cross-section per unit volume is calculated as the absolute square of the scattering amplitude:

$$\frac{d\Sigma\ (q,\alpha,\phi)}{d\Omega} = n|A_{nd}|^2 = n\Delta b_{nd}^2 P_{nd}(q,\alpha,\phi) \quad (10)$$

where $P_{nd}(q,\alpha,\phi)$ is written as an explicit function of α and ϕ as this is the form factor of a model nanodisc with a certain orientation. In order to calculate the form factor of randomly oriented particles an orientational average of $P_{nd}(q,\alpha,\phi)$ has to be done:

$$P_{nd}(q) = \frac{2}{\pi}\int_0^{\frac{\pi}{2}}\int_0^{\frac{\pi}{2}} |\psi_{nd}|^2 d\phi \sin(\alpha) d\alpha \quad (11)$$

This orientational averaging has to be performed numerically.

Refinement of the form factor

As it will be discussed later, this basic model presented above does not describe the experimental data satisfactorily. Therefore the model is refined two ways: First, the protein belts that surround the phospholipid bilayer are known to have a poly histidine tag (his-tag) each. This his-tag is constituted by 22 amino acid (7 histidines and an amino acid spacer domain) and may in a first approximation be modeled as Gaussian random coils attached to the outer rim of the MSP-belts. Secondly, the interface roughness observed in real experimental systems is incorporated into the model, so that the infinitely sharp interfaces of the cylinder model are smoothened according to a Gaussian distribution for the surface roughness.

Inclusion of the scattering from the His-tags. As will be discussed later and as demonstrated in Fig. 5 and 7 it is clear that the protruding his tags are visible in the data and have to be taken explicitly into account. The normalized form factor of the basic nanodisc model with two his-tags in the form of Gaussian random coils with excess scattering lengths Δb_c attached to the outer rim of the belt can be written as the sum of the following four terms:[15–17]

$$P(q) = \frac{(\Delta b_{nd}^2 P_{nd} + 2^2 \Delta b_c \Delta b_{nd} S_{nc} + 2\Delta b_c^2 S_{cc} + 2\Delta b_c^2 P_c)}{\Delta b_{\text{total}}^2} \quad (12)$$

where P_{nd} is the basic nanodisc model form factor (disc-disc self correlation), S_{nc} describe the interference between the nanodisc and the tags (disc-chain cross correlation), S_{cc} describes the interference between the tags (chain-chain cross

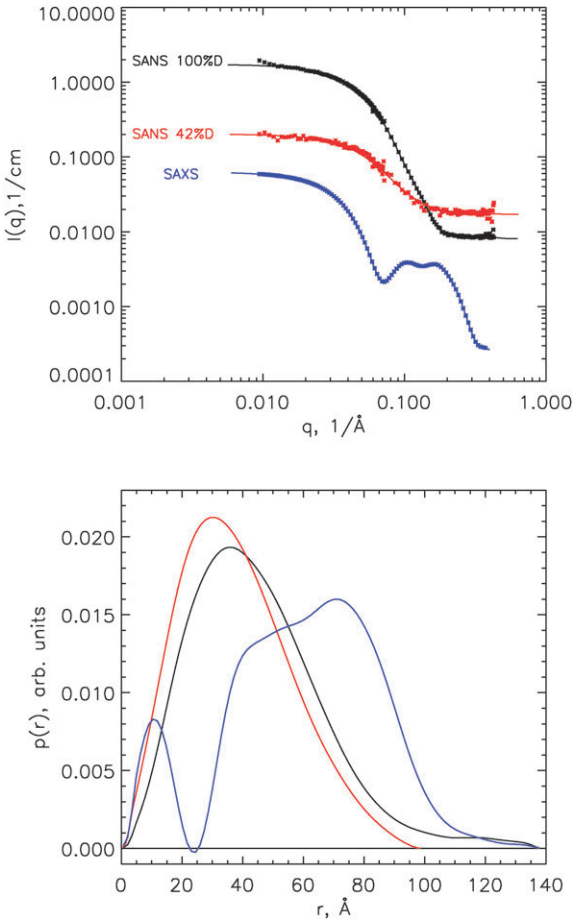

Fig. 5 (Top): SANS and SAXS data from the DLPC nanodiscs. SANS data are measured both in 100% D_2O and in 42% D_2O. (Bottom): The corresponding $p(r)$-functions.

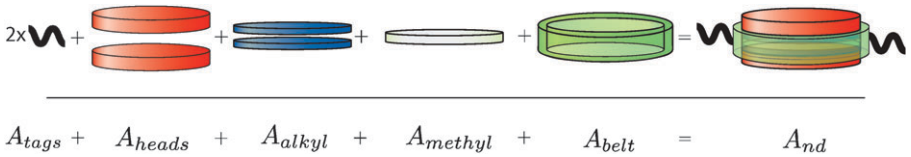

Fig. 4 Principle of assembling the entire nanodisc form factor.

correlation) and P_c describes the contributions from the single chain (chain-chain self correlation).

P_c is the form factor for a Gaussian random chain:[18]

$$P_c(q) = \frac{2(e^{-R_g^2q^2} + R_g^2q^2 - 1)}{R_g^2q^2} \quad (13)$$

where R_g is the radius of gyration of the Gaussian random chains.

Since the exact positions of the his-tags are unknown, and since we do not expect to have the structural resolution to locate them, we simply assume that they are uniformly distributed on the outer rim of he nanodisc belts. Under this assumption, the chain–chain and the disc-chain correlation terms of the Gaussian random chains attached to the disc become:[16]

$$P_{cc}(q,\alpha,\phi) = \left[\frac{1 - e^{-R_g^2q^2}}{R_g^2q^2}\right]^2 \times \left[J_0(q(R_o(\phi) + R_g)\sin(\alpha))\frac{\sin\left(q\frac{L}{2}\cos(\alpha)\right)}{q\frac{L}{2}\cos(\alpha)}\right]^2 \quad (14)$$

$$S_{nc}(q,\alpha,\phi) = \left[\frac{1 - e^{-R_g^2q^2}}{R_g^2q^2}\right] \times \left[J_0(q(R_o(\phi) + R_g)\sin(\alpha))\frac{\sin\left(q\frac{L}{2}\cos(\alpha)\right)}{q\frac{L}{2}\cos(\alpha)}\right]\psi_{nd} \quad (15)$$

where $R_o(a,b,\phi) = \sqrt{a_o^2\sin^2(\phi) + b_o^2\cos^2(\phi)}$ and L is the height of the belt. Note that, in eqn (14) and eqn (14), we have chosen to displace the center of mass of the his-tags a distance of R_g away from the outer rim of the belt. This is done in order to minimize the nonphysical overlap-clashes between the his-tags and the belt, *i.e.* to secure that space is only filled once.

As usual, the final form factor has to be orientational averaged over ϕ and α:

$$P(q) = \frac{1}{\Delta b_{\text{total}}^2}\int_0^{\frac{\pi}{2}}\int_0^{\frac{\pi}{2}}(\Delta b_{nd}^2P_{nd} + 4\Delta b_c\Delta b_{nd}S_{nc} + 2\Delta b_c^2S_{cc} + 2\Delta b_c^2P_c)\mathrm{d}\phi\sin(\alpha)\mathrm{d}\alpha \quad (16)$$

Inclusion of the interfacial roughness of the nanodiscs. The infinitely sharp interfaces of the analytical model results in some nonphysical artifacts at the high q part of the scattering curve. In order to remedy this, an average Gaussian distributed interface roughness is included in the model.[19] This is done by multiplying the obtained the final differential scattering cross-section by a Gaussian function: $P_{\text{final}}(q) = P(q)e^{-(q\sigma_i)^2/2}$ where σ_i is a measure for the interface roughness. It is important to note that this roughness parameter is an average roughness of all interfaces in the model and therefore can not be directly related to a specific interface. The importance of this term is clearly illustrated in Fig. 6(c) and turned out to be absolutely crucial to obtain good simultaneous fits to the SANS and SAXS data.

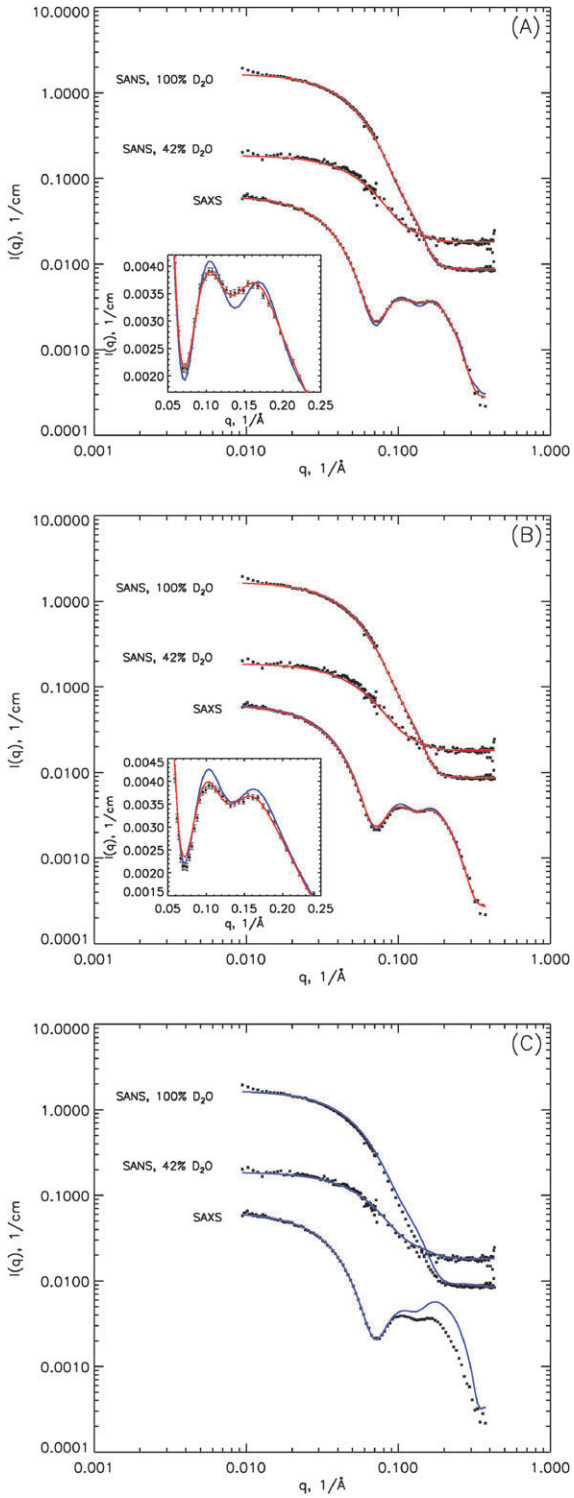

Fig. 6 Refinement of the modelling for the DLPC nanodiscs. Points: experimental data (see caption to Fig. 5). Full curves: The different iterations of the model for the DLPC-nanodiscs. (A) Effect of elliptical (red) *versus* circular (blue) nanodiscs. (B) Effect of not including the protruding His-tags. Blue: No his-tag but otherwise same model parameters as (red) elliptical model in (A). Red: Best fit with model without His-tag. (C) Effect of not including the surface roughness in the model.

Approach for the incorporation of molecular constraints

The underlying idea of including molecular constraints is to minimize the number of free parameters in the structural model and constrain the model fits to the relatively small subset of models that are physically realizable from the known molecular building blocks and which are furthermore consistent with the combined knowledge about the absolute scale of the different sets of scattering data along with other biophysical information, such as *e.g.* sample concentration and composition.

The particle number density. The particle number density is directly proportional to the protein concentration. As mentioned previously, nanodiscs consist of a protein belt and an interior phospholipid bilayer. It is generally accepted that the nanodisc protein belt consists of 2 MSP proteins[2] and a number of phospholipids which varies with the phospholipid type. The MSP concentration, in terms of moles per liter, M, may be accurately determined by a simple UV-absorption measurement for a given sample. Assuming two MSP's per nanodisc, the particle number density, n, is then easily calculated as $n = M/2 \cdot N_{\mathrm{lipid}}$, where N_{lipid} is the number of phospholipids per nanodisc. The lipid-concentration is notoriously more elaborate to determine with high accuracy from standard biophysical methods. In the present work this value has therefore been taken as a fit parameter *via* the fitting of the lipid-to-belt stoichiometry, N_{lipid}, of the single nanodiscs.

The phospholipid bilayer. In our model the phospholipid bilayer is modeled as a vertically symmetric stack of pairs of elliptically shaped cylindrical discs, where each cylindrical disc represents a different region of the phospholipid bilayer. The total volume of each pair of cylinders may be directly related to the partial specific molecular volume of the corresponding part of the phospholipid *via* N_{lipid}. Likewise, the total scattering length of each pair of cylindrical discs is directly calculated from the scattering length of the corresponding part of the phospholipid molecule times N_{lipid}. The scattering lengths and partial specific molecular volumes required for this calculation are listed in Table 1.

For example, the two methyl groups at the end of the hydrophobic phospholipid tails are estimated to have a partial specific molecular volume of $v_{\mathrm{meth}} = 108$ Å^3,[20] giving a total methyl volume of the methyl bilayer of $V_{\mathrm{methyls}} = N_{\mathrm{lipid}} v_{\mathrm{meth}}$. As each methyl group contributes to the scattering with 9 electrons, the total scattering length (for SAXS) of the cylinder representing the methyls is $b_{\mathrm{methyls}} = N_{\mathrm{lipid}} \cdot 9 r_0$, where r_0 is the Thompson scattering length. The excess scattering length of the methyl groups, $\Delta b_{\mathrm{methyls}}$, is $(b_{\mathrm{methyls}}/V_{\mathrm{methyls}} - \rho_0) \times V_{\mathrm{methyls}}$ which may also be calculated on the molecular level: $(9r_0/v_{\mathrm{methyls}} - \rho_0) \times v_{\mathrm{methyls}}$. From this we note that the excess scattering length density is dependent of the partial specific molecular volumes.

As a first estimate, the total partial specific molecular volume of the DLPC phospholipids in the bilayer is set to $v_{\mathrm{dlpc}} = 985$ Å^3. This value was obtained from high precision densitometry measurements involving radioactively labelled phospholipids for the accurate determination of sample concentration.[8] In order to quantify the molecular volume of the different parts of the DLPC we used a previously reported molecular volume of the PC head group of $v_{\mathrm{pc}} = 319$ Å^3.[21] The molecular volume of the alkyl chains then becomes: $v_{\mathrm{alkyl}} = v_{\mathrm{dlpc}} - v_{\mathrm{pc}} - v_{\mathrm{meth}}$.

The phospholipid head groups are hydrophilic and the model allows for the incorporation of a number of hydration water molecules associated with each PC group, N_w. These hydration water molecules will contribute to the volume of the cylinders representing the phospholipid heads, but not to the excess scattering length as they are assumed to have the same scattering length density as the solvent.

The DLPC area per head group, A_{head}, (*i.e.* the mean surface area taken up by one phospholipid molecule in the bilayer plane) is also taken as a fit parameter. From the combination of A_{head} and the partial specific molecular volume of the different molecular constituents of the phospholipid, the height of each part of the phospholipid lipid bilayer disc is easily calculated.

The axis ratio of the bilayer disc, $\varepsilon = a/b$ (see Fig. 2), is also taken as a fit-parameter.

The size and shape of the phospholipid bilayer is then determined by only four parameters: The aggregation number N_{agg}, the number of hydration water molecules per lipid N_w, the area per phospholipid A_{lip} and the cross-section axis ratio ε.

The membrane scaffolding protein belt. Our *a priori* estimate for the molecular volumes of the two scaffolding protein belts surrounding the phospholipid bilayer, is calculated using an average mass density of proteins of 1.356 cm^2/g.[22] The inner shape of the hollow cylinder describing the protein belt is constrained to the same shape as the phospholipid bilayer it surrounds. As the volume is fixed, the height of the belt, h_{belt}, is the only other parameter needed to describe the protein belt. The volumes of the two his-tags (22 amino acids each) is calculated using the same mass density and only their radius of gyration, R_g is a free fit parameter. The scattering length of the protein belt including the his-tags is determined from the MSP amino acid composition. And, using a similar approach as described above, the excess scattering length of the MSP becomes $\Delta b_{\mathrm{MSP}} = (b_{\mathrm{MSP}}/v_{\mathrm{mSP}} - \rho_0) - v_{\mathrm{msp}}$.

Adjustments to the molecular constraints. Because of the complex contrast situation in the SAXS experiment, with positive and negative excess scattering length densities in different domains of the nanodiscs, the model is extremely sensitive to minor deviation of the partial specific molecular volumes from the *a priori* values. Therefore adjustment parameters to be multiplied to the partial specific molecular volume of the DLPC and MSP were introduced. These parameters also allows the study of fine but experimentally anticipated thermal expansion or contraction when heating or cooling the sample. In any case, however, these volume correction-factors should be close to unity.

As a final free parameter, a constant can be added to the model scattering in order to correct for errors in the background subtraction, this parameter should be close zero.

Table 1 List of initial scattering lengths per molecule and partial molecular specific volumes used as molecular constraints

	Formula	b_{SAXS} [cm]	b_{SANS} [cm] in 100% D_2O	b_{SANS} [cm] in 42% D_2O	v [Å^3]
MSP belt	—	3.34×10^{-09}	8.27×10^{-10}	6.50×10^{-10}	27 588
MSP tag	—	3.87×10^{-10}	9.58×10^{-11}	7.52×10^{-11}	3194
DLPC head	$C_{10}H_{18}NO_8P$	4.62×10^{-11}	7.05×10^{-12}	7.05×10^{-12}	319
DLPC alkyl	$C_{20}H_{40}$	4.51×10^{-11}	-1.67×10^{-12}	-1.67×10^{-12}	557
DLPC methyl	C_2H_6	5.08×10^{-12}	-9.15×10^{-13}	-9.15×10^{-13}	108.6
H_2O	H_2O	2.82×10^{-12}	-1.68×10^{-13}	-1.68×10^{-13}	30.0
D_2O	D_2O	2.82×10^{-12}	1.91×10^{-12}	1.91×10^{-12}	30.0

Results and discussion

Visual inspection of the experimental scattering intensities and pair-distance distribution functions

DLPC-nanodiscs were measured by SANS and SAXS in two SANS contrast situations, respectively, 100% D_2O buffer and 42% D_2O/58% H_2O buffer, as well as in the ordinary SAXS contrast obtained in 100% aqueous buffer. An example of the obtained scattering data along with the corresponding pair-distance distribution functions, $p(r)$, are plotted in Fig. 5. The sample concentrations for the SAXS sample and SANS sample in 100% D_2O sample was 3.2 mg/ml. This corresponds to a nanodisc concentration of 23.0 μM. The SANS sample in 42% D_2O had a sample concentration of 5.5 mg/ml, corresponding to 38.5 μM nanodiscs.

The 100% D_2O SANS contrast is a bulk contrast with significant negative excess scattering length densities for both protein belt and phospholipid core. The protein belt is matched out to zero excess scattering length density in the 42% D_2O SANS contrast, making only the phospholipid core visible. Both SANS data set exhibit a monotonically decaying differential scattering cross-section. In the SAXS contrast situation, the hydrophobic part of the phospholipid core has negative excess scattering length density, whereas both the phospholipid headgroups and the protein belt has positive excess scattering length densities. This inhomogeneous contrast with both positive and negative contributions to the scattering amplitudes gives rise to the very significant oscillating behavior of the SAXS scattering intensity comparable to what is *e.g.* observed in surfactant micelle systems.

The $p(r)$ functions were calculated using an implementation of Glatters original IFT-procedure.[10] We used a Fortran implementation of the routine (originally programmed by Prof. Jan Skov Pedersen) that had a slightly modified smoothness constraint.[23] In the $p(r)$ plot in Fig. 5, the $p(r)$-functions are normalized such that the area under the $p(r)$-function becomes unity.

The $p(r)$-function of the SANS 100% D_2O contrast has a slightly skewed, but otherwise bell-shaped $p(r)$-function. A tail is clearly visible at r-values in the interval from 100 Å to 140 Å. This behaviour is consistent with our expectations to the shape of the nanodiscs as being small compact discs with his-tags protruding out from the outer rim of the belts that stabilize the sides of the discs. The $p(r)$-function of the SANS 42% D_2O contrast has a similar shape as that of the SANS 100% D_2O contrast. However, in 42% D_2O, both the maximum value of the $p(r)$ and the D_{max} are clearly shifted to lower values, and in particular the tail at high r-values is not present. This is all a result of the contrast matching of the protein belt, which is then no longer visible. Instead the smaller hydrophobic part of the lipid bilayer almost exclusively dominates the scattering pattern and the $p(r)$-function. In the SAXS contrast, where, as mentioned above, an oscillating differential scattering cross-section is obtained as a result of the combination of the negative excess scattering length density in the hydrophobic core and positive excess scattering length density in both the hydrophilic head-groups and the protein-belt, we also obtain a non-monotonic behavior of the $p(r)$-function. The D_{max} is similar to that obtained in the SANS 100% D_2O contrast and again we observe a tail at high r-values which is most likely a signature of the protruding his-tags. Due to the totally different SAXS contrast situation, the remaining part of the $p(r)$-curve differs significantly from those obtained in the other two contrast situations. The comparison between the three illustrates very clearly the value of combining SANS and SAXS.

Refinement of the structural model for the nanodiscs

The data from the two SANS contrasts and the single SAXS contrast were fitted simultaneously by minimizing the reduced χ^2 using the model for nanodiscs with elliptical cross-section with protruding his-tags in a Gaussian random coil conformation described in section "Theory and mathematical Modeling". As shown in Fig. 6(A) an excellent agreement ($\chi^2 = 1.85$) is obtained between model and experimental data when using a model for nanodiscs with an elliptical cross-section and protruding his-tags in a Gaussian random coil conformation, whereas significant systematic deviations between model and data are obtained along with a higher reduced χ^2 of 2.36 is obtained when the nanodiscs are forced into the previously suggested consensus model for nanodiscs with a circular cross-section.[2,3,24]

As a part of the model-refinement process several more simple models were investigated. The effect of including the his-tags explicitly as protruding Gaussian random coils attached to the outer rim of the MSP-belts is investigated in Fig. 6(B). The blue curve is a model calculation using the same model parameters as in the elliptical model fit (red curve) shown in Fig. 6(A) except that the his-tag is now omitted and the corresponding mass instead assumed evenly distributed in the protein belt. Without any fitting this gives rise to large and systematic deviations and an increase of the χ^2 to 5.94. After fitting of the remaining parameters we obtained the red curve of Fig. 6(B) which is the best fit that may be obtained with the model without his-tag. The over-all fit is good ($\chi^2 = 2.71$), however, significant

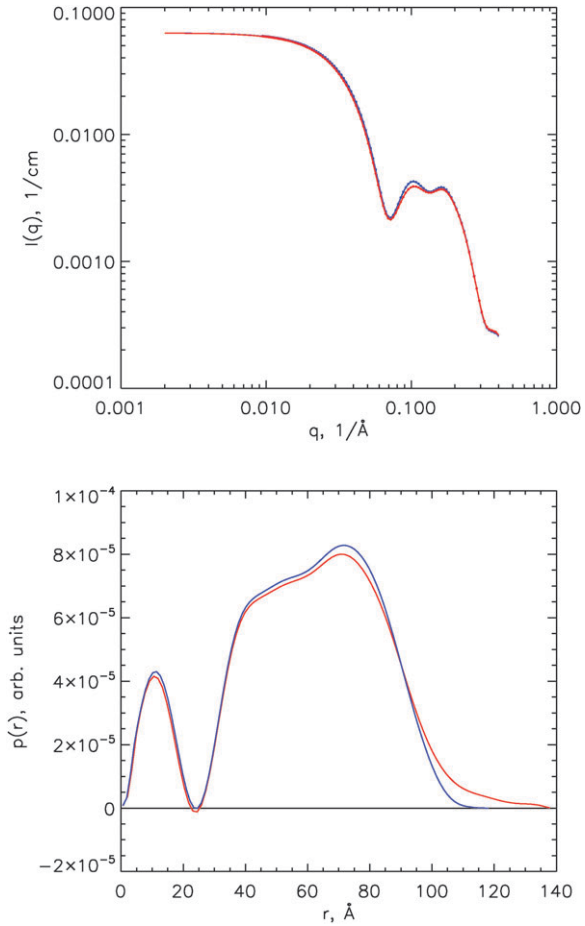

Fig. 7 (Top): Analytical SAXS differential scattering cross-sections for the DLPC nanodiscs. Red: Model for nanodiscs with protruding his-tags. Blue: Model for nanodiscs without his-tags. (Bottom): The corresponding $p(r)$-functions (same colour-code).

systematic deviations around the first minimum in the SAXS curve are clearly visible.

To further elucidate the effect of the his-tags on the differential scattering cross-sections, the model calculations for the nanodiscs, with and without his-tag, are plotted in Fig. 7 without the experimental data. Only the model calculation corresponding to the SAXS contrast is plotted here. As seen, the effect of removing the his-tag is visible in the scattering data. However, the effect is difficult to interpret from the differential scattering cross-sections alone. This situation changes in the $p(r)$-representation of the analytical scattering cross-section (also plotted in Fig. 7), where the effect of the protruding his-tags is very clearly seen as a significant tail at high r-values. This clearly illustrates the advantage of plotting small-angle scattering data both in their reciprocal space and direct space representations. It also gives strong support to the interpretation of the comparable tails observed in the $p(r)$ functions determined from our experimental data Fig. 5.

In Fig. 6(C) the effect of *not* including the roughness term is shown. The blue curve is the small-angle scattering calculated for the same model parameters as for the elliptical nanodiscs (red curve) in Fig. 6(A) however the surface roughness is set to zero corresponding to infinitely smooth interfaces between the different inner and outer layers of the nanodisc. While this model is clearly nonphysical it also gives rise to a really poor agreement between model and data. Clear deviations between model and data already sets in before $q = 0.001$ 1/Å and the over-all χ^2 increases to 100. It was attempted to obtain a better fit. However, while a significantly lower χ^2 could be obtained (lowest χ^2 was about 25), large systematic deviations remained clearly visible and the fit did not converge satisfactorily.

Table 2 Results from the simultaneous fits to SANS and SAXS data on DLPC nanodiscs at 20 °C. The "Fitting parameters" are the parameters determined directly by the fits. "Deduced parameters" are derived from the fitted parameters as a consequence of the molecular constraints imposed on the model

Fit parameters:	DLPC, N/X T = 20 °C
N_{DLPC}	150 ± 1
ε	1.29 ± 0.02
A_{head}, Å^2	58.6 ± 0.2
N_w	0.0[a]
ν_{DLPC}, Å^3	997.5 ± 0.4
ν_{MSP}, Å^3	30217 ± 33
H_b, Å	24.0[a]
R_g, Å	12.7 ± 0.7
$\sigma_{roughness,X}$, Å	4.24 ± 0.04
$\sigma_{roughness,N}$, Å	4.58 ± 0.18
Deduced parameters:	
H_{total}, Å	34.0 ± 0.1
$H_{Hydrophobic}$, Å	23.0 ± 0.1
A_{disc}, Å^2	4408 ± 13
D_{minor}, Å	65.9 ± 0.7
D_{major}, Å	85.1 ± 1.4
d_{belt}, Å	8.5 ± 0.8

[a] Parameter not fitted. N_{DLPC}: The number of DLPC's per nanodisc, ε: Axis ratio of lipid core, A_{head}: Area of the PC head group, N_w: Hydration number, ν_{PC}: Partial specific molecular volumes of the phospholipid. ν_{MSP}: Partial specific molecular volume of the MSP (*i.e.* the sum MSP belt and MSP his-tag). Note that H_b: Height of the MSP-belt, R_g: Radius of gyration of the his tags, $\sigma_{roughness,X}$: Average interface roughness as observed in the SAXS contrast, $\sigma_{roughness,N}$: Average interface roughness as observed in the SANS contrast. A_{disc}: Total area of the phospholipid part of the disc. H_{Total}: Total height of the phospholipid bilayer. $H_{Hydrophobic}$: Height of hydrophobic bilayer. D_{minor} and D_{major}: Minor and major diameter of the phospholipid bilayer. d_{belt}: Thickness of the MSP-belt.

The fit parameters corresponding to the best fit, plotted in Fig. 6a (red), are summarized in Table 2. In the upper half of the table, the actual fit parameters are listed. Whereas in the lower half, those structural parameters are listed that, due the systematic use of molecular constraints, are deduced from the fit parameters.

Over-all shape of the nanodiscs. We find that the nanodiscs have a significant elliptical shape with an axis ratio of 1.29 and an average number of DLPC's per nanodisc of 150. One of the central dogma in small-angle scattering is that the effect of polydispersity and the effect of deviating from sphero-symmetry can not be distinguished. While there is already both theoretical[25] and experimental[19] evidence that speaks against this dogma, one should definitely be careful when trying to distinguish between the two effects and quantify them separately. In the nanodisc system, however, the case is somewhat more simple as the constant circumference of the MSP-belt gives strong restrictions to how polydisperse the nanodiscs may be. To first order and assuming a fixed area

per headgroup of the phospholipids, only a dispersity in terms of the number of DLPC molecules per nanodisc, N_{DLPC}, is allowed. This has the consequence that perfectly circular discs are automatically also monodisperse, whereas a dispersion in N_{DLPC} will give rise to an, on average elliptical, shape of the nanodisc-cross-section. It may however be questioned to what extent the maximally loaded circular discs are favoured entropically. Simple statistical mechanical arguments[8] along with experimental evidence for much faster lipid exchange in nanodiscs as compared to liposomes[24] strongly supports that the thermodynamically favoured state of the nanodiscs will be a state where the belt is not maximally expanded and the disc has an elliptical shape. As this elliptical shape will always provide the leading contribution to the smearing of the differential scattering cross-section, an elliptical rather than a polydisperse (spherical) shape was implemented already in the early stages of the model refinement-process. In the process of data analysis and model refinement, a dispersion in the N_{DLPC} was also implemented in terms of a (truncated) Gaussian distribution number of DLPC's per nanodisc around the average N_{DLPC}. This introduced the width of the Gaussian, $\sigma_{N\text{-DLPC}}$, as an extra fit-parameter, however, when $\sigma_{N\text{-DLPC}}$ was fitted, it very quickly decreased towards a value corresponding to zero dispersion. While this is not a proof that the nanodiscs are elliptical and fully monodisperse, it definitely suggests, that the dispersion in N_{DLPC} is rather small.

The packing of the molecular constituents of the nanodiscs. The obtained A_{head} of 58.6 Å^2 for DLPC in nanodiscs is comparable to the value observed in phospholipid bilayer liposomes.[26] However, as it is being discussed and documented in more detail in ref. 8, the area is slightly smaller than the liposome value, and consistent with a lateral compression of the DLPC bilayer when this is localized in a nanodisc. The data suggest that the number of water molecules per PC headgroup, N_w, is very low in the system. Indeed, when the N_w was fitted, it ended up very close to zero and in practice we decided to fix the N_w to zero in the simultaneous fit in order to avoid nonphysical minima with a slightly negative N_w-value. As mentioned previously, we have very good estimates for the partial specific molecular volumes of the DLPC and the MSP, but do not know these values in the nanodiscs with 100% certainty. For this reason these values were taken as adjustment parameters. While the effect of slightly adjusting the partial specific molecular volumes is general non-significant in the fitting of the bulk-like SANS-contrasts, the fine-tuning of these play a remarkably central role for obtaining a good fit to the SAXS data. In the nanodiscs we observe a ν_{DLPC} of 998 Å^3 and a ν_{MSP} of 30220 Å^3. For the DLPC, the obtained value should be compared to the value of 985 Å^3 that we have observed by densitometry measurements in multilamellar liposome systems (see ref. 8), whereas for the MSP the observed molecular volume corresponds to a mass-density of 1.362 g/cm^3 in very close agreement with the value of 1.347 g/cm^3 reported as a representative average value for a wide range of different sized protein systems.[22]

Interface roughness of the nanodiscs. As mentioned above and illustrated in Fig. 6(C), the effect of explicitly including the interfacial roughness of the nanodiscs is very significant. The data from the three contrast could not be fitted simultaneously without explicitly including the roughness term, while excellent fits was obtained when including this term. In both the SAXS and the SANS contrasts we find a surface roughness slightly above 4 Å. This roughness is slightly higher than what we have previously observed in a droplet microemulsion system,[19] but not surprising when taking into account the relatively rough peptide interface as defined by the MSP-belts and when considering that we are describing the alphahelical MSP-belt by an edged hollow cylinder.

Conclusion

A detailed structural model for nanodiscs is derived and refined against experimental SANS and SAXS data obtained on a DLPC-nanodisc sample measured at 20 °C. The systematic incorporation of additional experimental information of molecular or biophysical character allow us to determine the solution structure of the nanodiscs with a so far, unprecedented structural resolution. Several smaller elements have to be combined in order to obtain a good and self-consistent structural model. One of the remarkable effects is the surface roughness term which is absolutely crucial to take into account, in particular when analysing high-resolution small-angle X-scattering data ($q_{max} \approx 0.5$ Å) that are becoming more and more widely accessible at Synchrotron SAXS beamlines optimized for solution scattering. In the present work, we succeed in giving a satisfactory description of the scattering data using a model based on "geometrical" building blocks. However, this approach has a limited resolution and we expect that the steadily improving high-q resolution at synchrotron SAXS instruments, will create a demand for more realistic descriptions of the molecular structures. This could be descriptions that explicitly include the molecular structure of the building blocks such that the short length scale density fluctuations and interface roughness present in alpha-helices, phospholipid bilayers *etc*. are automatically taken into account. This approach will also potentially enable the inclusion of non-symmetric objects such as membrane proteins, which can only in a very crude approximation be described *via* a geometrical object.

Experimental

Preparation of nanodiscs

The preparation of studied nanodisc samples are fully described in ref. 8 and follows the standard procedures previously documented.[1]

SAXS and SANS measurements

SANS and SAXS data sets for the simultaneous analysis (Fig. 6) were acquired at, respectively, the SANS instrument D11 at Institut Laue Langevin (ILL) and at the Bio-SAXS instrument at beamline ID14-3 at European Synchrotron Radiation Facility (ESRF). Both facilities are located in Grenoble, France. For the SANS measurements a combination of two instrumental settings were used to obtain

a sufficiently wide q-range: A setting for covering the high q-values with a sample-detector distance of 1.5 m, and a collimation length of 4 m and a setting for covering the medium q-values with a sample-detector distance of 4 m, and a collimation length of 10.5 m. In both cases a neutron wavelength of 6.0 Å was used with a wavelength spread, $\Delta\lambda/\lambda$ of 10% FWHM. Both the SANS and SAXS measurements were performed at 20 °C. Absolute scale calibration was performed using H_2O as external reference and following the standard procedures at the facility. All samples were measured in flat rectangular Hellma quartz cells during the measurements. In order to optimise signal-to-noise and minimize incoherent background and multiple scattering effects, the samples in 100% D_2O were measured in cells with a path length of 2 mm, whereas the samples in 42% D_2O/58% H_2O was measured in cells with a path length of 1 mm. For the SAXS measurements we used the fixed instrument setup including the HPLC-based automatic sample loading robot standard to the beamline ID14-3. Here the path length of the sample cell was 1 mm. Absolute scale calibration was performed using Bovine Serum Albumin as the external reference.

The SANS measurements were performed two days prior to the SAXS measurements. Ahead of the SANS measurements, the usual H_2O-based buffer used in the nanodisc preparation, had been substituted for corresponding buffers with, respectively 100% D_2O and 42% D_2O/58% H_2O. In the latter contrast, the membrane scaffolding protein is contrast matched and in practice invisible in the experiments. The isotope substitution of the buffers was performed using centrifugal spin-filters with a cut-off of 100 kDa.

Small resolution effects are present in the SANS data, mainly due to the non-negligible spread of the wavelengths of the incoming neutrons. In the synchrotron SAXS data, resolution effects are in practice negligible due to a very high monochromaticity of the incoming beam, a very small beam-diameter and a close to perfect collimation. The resolution effects may easily be included in the data analysis following the principles described in ref. 27 by smearing the model function by the appropriate resolution function before comparing model to experimental data. The inclusion of the resolution function typically affects the fit results, however, in the present case, and with the good resolution obtained at D11 at ILL, the effects were in practice fully negligible; neither the reduced χ^2 or the fit-results were affected. As an exception to usual procedures, the resolution effects were therefore not included in order to gain computational speed.

Acknowledgements

The authors thank Dr A. Round at the ID14-3 Bio-SAXS beamline at ESRF, the European Synchrotron Radiation Facility and Dr R. Schweins at the SANS instrument at beamline D11 at ILL, Institute Laue Langevin. In particular, we gratefully acknowledge the access to "simultaneous" SAXS and SANS beamtime at ILL and ESRF. The authors also wish to thank Prof. Steven Sligar and the Sligar-lab for providing us with MSP1D1 for the nanodiscs. Finally we thank the Danish Government funded UNIK Synthetic Biology program for co-funding of the project and the Danish Research Council funded Danscatt-organization for providing economical support to travels to large facility SAXS and SANS beam time.

References

1 T. H. Bayburt, Y. V. Grinkova and S. G. Sligar, *Nano Lett.*, 2002, **2**, 853–856.
2 I. G. Denisov, Y. V. Grinkova, A. Lazarides and S. G. Sligar, *J. Am. Chem. Soc.*, 2004, **126**, 3477–3487.
3 I. G. Denisov, M. McLean, A. Shaw, Y. V. Grinkova and S. G. Sligar, *J. Phys. Chem. B*, 2005, **109**, 15580–15588.
4 T. H. Bayburt, Y. V. Grinkova and S. G. Sligar, *Arch. Biochem. Biophys.*, 2006, **450**, 215–222.
5 M. R. Whorton, M. P. Bokoch, S. G. F. Rasmussena, B. Huang, R. N. Zare, B. Kobilka and R. K. Sunahara, *Proc. Natl. Acad. Sci. U. S. A.*, 2007, **104**, 7682–7687.
6 T. H. Bayburt and S. G. Sligar, *FEBS Lett.*, 2010, **584**, 1721–1727.
7 A. Y. Shih, I. G. Denisov, J. Phillips, S. G. Sligar and K. Schulten, *Biophys. J.*, 2005, **88**, 548–556.
8 N. Skar-Gislinge, J. B. Simonsen, K. Mortensen, R. Feidenhans'l, S. G. Sligar, B. L. Møller, T. Bjørnholm and L. Arleth, *J. Am. Chem. Soc.*, 2010, **132**, 13713–13722.
9 O. Mouritsen and M. Bloom, *Biophys. J.*, 1984, **46**, 141–153.
10 O. Glatter, *J. Appl. Crystallogr.*, 1977, **10**, 415–421.
11 F. Ye, G. Hu, D. Taylor, B. Ratnikov, A. A. Bobkov, M. A. Mclean, S. G. Sligar, K. A. Taylor and M. H. Ginsberg, *J. Cell Biol.*, 2010, **188**, 157–173.
12 J. S. Pedersen and C. Svaneborg, *Curr. Opin. Colloid Interface Sci.*, 2002, **7**, 158–166.
13 J. S. Pedersen, *Adv. Colloid Interface Sci.*, 1997, **70**, 171–210.
14 J. S. Pedersen, in *Neutrons, X-rays and Light: Scattering Methods Applied to Soft Condensed Matter*, ed. P. Linder and T. Zemb, Elsevier Science B. V., Amsterdam, 2002, ch. 16.
15 J. S. Pedersen and M. Gerstenberg, *Macromolecules*, 1996, **29**, 1363–1365.
16 J. S. Pedersen, *J. Appl. Crystallogr.*, 2000, **33**, 637–640.
17 L. Arleth, B. Ashok, H. Onyuksel, P. Thiyagarajan, J. Jacob and R. Hjelm, *Langmuir*, 2005, **21**, 3279–3290.
18 P. Debye, *J. Phys. Chem.*, 1947, **51**, 18–32.
19 L. Arleth and J. S. Pedersen, *Phys. Rev. E*, 2001, **63**, 061406.
20 C. Tanford, *J. Phys. Chem.*, 1972, **76**, 3020–3024.
21 W. Sun, R. Suter, M. Knewtson, C. Worthington, S. Tristram-Nagle, R. Zhang and J. F. Nagle, *Phys. Rev. E*, 1994, **49**, 4665–4676.
22 E. Mylonas and D. I. Svergun, *J. Appl. Crystallogr.*, 2007, **40**, 245–249.
23 J. S. Pedersen, S. L. Hansen and R. Bauer, *Eur. Biophys. J.*, 1994, **22**, 379–389.
24 M. Nakano, M. Fukuda, T. Kudo, M. Miyazaki, Y. Wada, N. Matsuzaki, H. Endo and T. Handa, *J. Am. Chem. Soc.*, 2009, **131**, 8308–8312.
25 E. Caponetti, M. Floriano, E. Didio and R. Triolo, *J. Appl. Crystallogr.*, 1993, **26**, 612–615.
26 Dr N. Kucerka, Personal communication cited with permission from N. K. Canadian Neutron Beam Centre, National Research Council of Canada Chalk River Laboratories, Chalk River, Canada.
27 J. S. Pedersen, D. Posselt and K. Mortensen, *J. Appl. Crystallogr.*, 1990, 321–333.

